ISSN 1392-1320 MATERIALS SCIENCE (MEDŽIAGOTYRA). Vol. 25, No. 3. 2019

Microstructure and Magnetic Studies of $La_{1-x}Sr_xFeO_3$ Nano Particles Fabricated by the Citrate Sol-Gel Method

Fang YANG [1, 2], Xing Xing YANG [2], Qing LIN [1, 2] *, Rui Jun WANG [1], Hu YANG [3], Yun HE [2, 3]

[1] *College of Medical Informatics, Hainan Medical University, Haikou 571199, P.R.China*
[2] *Guangxi Key Laboratory of Nuclear Physics and Nuclear Technology, Guangxi Normal University, Guilin 541004, P.R.China*
[3] *College of Physics and Technology, Guangxi Normal University, Guilin 541004, P.R.China*

crossref http://dx.doi.org/10.5755/j01.ms.25.3.19455

Received 10 November 2017; accepted 06 April 2018

The paper reports the use the sol-gel auto-combustion method for the preparation of nanocrystalline $La_{1-x}Sr_xFeO_3$ (x = 0÷0.7). The physical and chemical properties, microstructure, morphology and magnetic properties of the particles thus formed were studied. The X-ray diffraction (XRD) results indicated that Sr^{2+} instead of perovskite La are attributed to the lattice forming solid solution $La_{1-x}Sr_xFeO_3$, which has single orthogonal perovskite structure, space group Pnma, and does not show any impurity peaks. Fourier-transform infrared (FT-IR) spectroscopy confirmed the presence of Fe-O-Fe bond antisymmetric stretching vibration of FeO_6 regular octahedron. The scanning electron microscope (SEM) analysis showed that introduction of Sr^{2+} ions can inhibit the growth of size of the particles thereby forming particles with spherical shape and better dispersion properties. The magnetic properties of the sample showed that with increase in Sr^{2+} ion concentration leads to increase in sample's magnetism.
Keywords: $LaFeO_3$, Sr^{3+} doping, citrate sol-gel, nanoparticle, magnetic properties.

1. INTRODUCTION

Perovskite-type (ABO_3) rare-earth metal oxide [1, 2] is a kind of new inorganic non-metal material that possesses unique physical and chemical properties. Lanthanum ferrite composite oxide nanopowder ($LaFeO_3$) are nano-scale particles of a material [3, 4], which possess unique magnetic, optical and electrical properties, that can be attributed to the congregation of multifactorial effects, such as small size effect, surface effect [5, 6]. The properties of these nanoparticles may sometimes vary from the macro-scale material itself [7, 8]. Their properties are based on that alkaline earth elements can replace the rare earth elements and change its crystal microstructure and electromagnetic properties. In this paper, the low temperature synthesis of perovskite type composite oxide nanoparticles $La_{1-x}Sr_xFeO_3$ through the citrate sol-gel method is reported. The effect of Sr^{2+} substitution $La_{1-x}Sr_xFeO_3$ nanoparticles the influence of Sr^{2+} substitution in magnetic properties and microstructure are investigated.

2. EXPERIMENTAL SECTION

2.1. Sample synthesis

This experiment by using citrate sol-gel synthesis $La_{1-x}Sr_xFeO_3$(x = 0÷0.7) powder, studied different proportions of Sr doped and calcination temperature for microstructure, morphology and magnetic properties of the samples. The desired quality of the sample was weighed sample $La(NO_3)_3{\cdot}6H_2O$, $Fe(NO_3)_3{\cdot}9H_2O$, $Sr(NO_3)_2$ and citric acid; citric acid dissolved in deionized water, to be completely dissolved before obtaining A solution; a variety of nitrate dissolved in citric acid solution A until completely to give B solution. Slowly adding ammonia was used to adjust B solution PH = 7 to obtain a sol. After putting sol at 60 ℃ and water bath pot stirring, sol becomes wet gel after about 3 h, then stirring was stopped. The wet gel was aged for about 12 h, placed blast oven 130 ℃ drying 6 h get xerogel. Accelerant (ethanol) was added to the dry gel from spread, to get mud yellow fluffy powder. Polishing powder was placed in a crucible, according to the required temperature and time, respectively, calcined in a muffle furnace.

2.2. Sample characterization

The integrated technique of thermogravimetric analysis and differential scanning calorimetry (TG-DSC) (SDT Q600, TA Instruments, USA) was used to analyze the dry gel through thermal decomposition process. In this experiment, X-ray diffraction (D/max-2500v/pc, Rigaku, Japan) was used to characterize the structure of the material: the main parameters of the X-ray diffraction process were as follows: accelerating voltage, 40 kV; electric current, 20 mA; Cu-Kα radiation; scanning speed is 10°/min; scanning range from 10° to 80° (2θ). Fourier transform infrared spectroscopy (FT-IR) (Spectrum Two; Perkin Elmer, USA) was performed to observe functional groups and chemical bonds of the samples. Then, infrared (IR) spectroscopic analysis of the samples was performed in the wavelength range of 400-4000 cm^{-1}. Scanning electron microscopy (NoVa™ Nano 430; FEI, USA) was used to observe the microstructural properties of $LaFeO_3$ nanomaterial, including particle size, geometrical shape, uniformity, and contact phenomenon. The magnetic character of the samples was tested with a vibrating sample

* Corresponding author. Tel.: +86-773-5840785; fax: +86-773-5811173.
E-mail address: *elinqing@126.com* (Q.Lin)

magnetometer (VSM-100) that was performed from the Changchun Tome Magnetoelectricity Technology Development Ltd, Jilin, China. We tested hysteresis loop of the samples at room temperature under the following conditions: the maximum magnetic field H = 0.8 T, and the highest sensitivity was 5×10^{-5} emu. With this process, we determined the magnetic parameters of samples, including the saturation magnetization (Ms), remnant magnetization (Mr), and coercive force (Hc) values.

3. RESULTS AND DISCUSSION

3.1. TG analysis

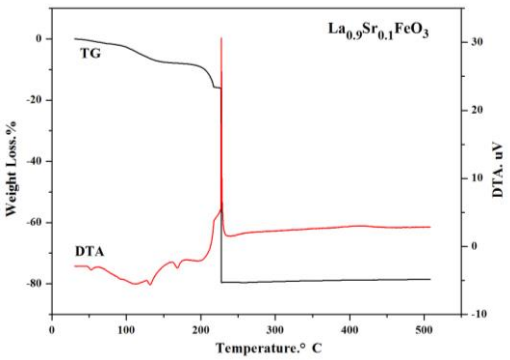

Fig. 1. TG and DTA curves of $La_{0.9}Sr_{0.1}FeO_3$ xerogel powder

The TG and DTA curves of $La_{0.9}Sr_{0.1}FeO_3$ xerogel powder are represented in Fig. 1. It can be seen that when the temperature rose from 30 ℃ to 228 ℃, the weight of xerogel slowly decreases. This change can be attributed to citric acid decomposition and the release of the adsorbed water of the sample and other volatile substances present in it [9 – 10]. The exothermic peak at 228 ℃, is extremely close to the temperature corresponding to maximum observed weightlessness in the TG curve, which is due to the heat combustion and release of the citric acid salt [11]. Additionally, the same temperature also corresponds to the oxidative decomposition of residual NO^{3-} [9]. As the temperature rises above 228 ℃, the TG curve tend to be stablized, which indicates that the $La_{1-x}Sr_xFeO_3$ compound oxide has reached its crystalline state. Indirectly, the TG curve revealed that the minimum temperature of preparation of completely crystallized nanocrystalline $La_{1-x}Sr_xFeO_3$ is 228 ℃.

3.2. XRD analysis

The XRD diffraction patterns of $La_{1-x}Sr_xFeO_3$(x = 0÷0.7) represented in Fig. 2 show that it did not calcine. Furthermore, the (121) peak drift figure of XRD patterns demonstrated that all the samples were of perovskite orthogonal structure with Pnma space group (62). Moreover, the diffraction peak of the sample corresponded to the standard peak of $LaFeO_3$ (No.37-1493 JCPDS). It was also observed that increase in Sr^{2+} doping concentration caused the diffraction peak intensity to abate. However, it still maintained its orthogonal structure with little or no modifications in the symmetry of crystal structure [3, 4]. Fig. 2 also shows peak shift as the Sr doping amount increases. As analyzed by the Bragg equation:

$$2d\sin\theta = n\lambda, \quad (1)$$

where d is the grain size, θ is the diffraction angle, λ is the X-ray wavelength.

The XRD spectrum diffraction peak shift is in the direction of high angle. Along with it, the crystal cell parameters show reduction, which means that the doping by Sr changes La atoms in the $LaFeO_3$ lattice and causes lattice distortion and cell shrinkage, thereby changing its physicochemical properties [9 – 11].

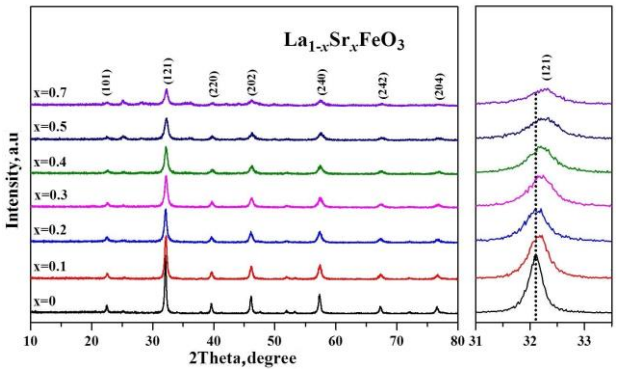

Fig. 2. XRD diffraction pattern of $La_{1-x}Sr_xFeO_3$(x=0÷0.7) which did not calcine and (121) peak drift figure

The lattice parameters changes during the analysis are listed in Table 1. It is shown that when $x \leq 0.5$, the cell volume decreased with increasing Sr doping concentration. Such behavior can be attributed to the changes in A bit size and Fe valence that are congruent with Sr alternation. These results were found to be contradictory, especially because Sr^{2+} ionic radius (0.144 nm) is larger than La^{3+} ionic radius (0.136 nm). This can be explained by the fact that as Sr^{2+} concentration increases, Fe^{3+} (ionic radius-0.0645 nm) gets oxidized to Fe^{4+} (ionic radius – 0.0585 nm) so that the electrically neutral nature of the whole compound is preserved [2].

Table 1. The lattice parameter of non-calcined $La_{1-x}Sr_xFeO_3$(x=0~0.7)

Content, x	a, Å	b, Å	c, Å	vol, Å^3	Density, g/cm^3	Crystallite, nm
0	5.56753	7.87365	5.56852	244.11	6.6053	28.6
0.1	5.57234	7.86790	5.55069	243.36	6.6256	20.7
0.2	5.54630	7.86803	5.57923	243.47	6.6225	16.3
0.3	5.55317	7.86374	5.56056	242.82	6.6402	16.2
0.4	5.54624	7.86581	5.55294	242.25	6.6558	14.0
0.5	5.54425	7.84253	5.55584	241.57	6.6745	12.5
0.7	5.62733	7.77571	5.58716	244.47	6.5953	14.7

Interestingly, as the Fe^{4+} proportion of the compound increases, the number of covalent interactions between Fe and O ions increase. This further enhances atomic orbital overlapping between Fe-O, thereby causing decrease in the cell volume [4]. Another factor that is known to affect cell volume is the oxygen content of the compound [12, 13]. When Sr doping amount increases, the perovskite structure produces oxygen vacancy [14, 15] which leads to cell volume change. Increase in volume was also detected when $x = 0.7$, which may be related to many factors, including internal stress, oxygen vacancy, the effects of surface energy and surface stress [3, 16]. According to the Scherrer's formula, particle size gets reduced, until the doping amount reaches 0.7, after which they tend to increase in size [5, 6].

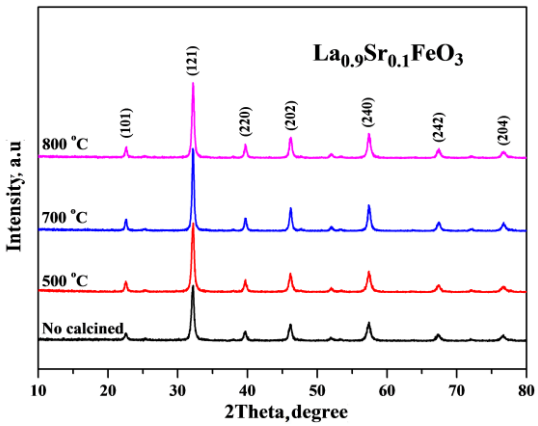

Fig. 3. XRD diffraction pattern of $La_{0.9}Sr_{0.1}FeO_3$ sample calcined at different temperatures

Fig. 3 represents the XRD diffraction pattern of $La_{0.9}Sr_{0.1}FeO_3$ calcined at different temperatures. The XRD patterns show that the main diffraction peak is consistent with the standard sample $LaFeO_3$ (JCPDS No. 37-1493) card. It also shows that no other phase is generated, and the space group is Pnma. Furthermore, the obtained peaks that are characteristic of the orthogonal structure indicate that the three kinds of calcination tend to immerse the Sr^{2+} in the crystal lattice of the perovskite [7].

The average grain size of the sample when $La_{0.9}Sr_{0.1}FeO_3$ was calcined at different temperatures, was found to be 19.3 nm, 20.7 nm, 26.4 nm and 23.0 nm, respectivelly (uncalcined, 500 ℃, 700 ℃, 800 ℃). The values indicate that they follow a trend of first decreasing and then increasing. As shown in Table 2, the diffraction peak half width were found to be 0.412, 0.431, 0.267, 0.130 respectively, which indicated that the values first tend of increase, then decrease [17, 18], which when calcining temperature is 700 ℃, the average grain size of sample is greater than 800 ℃ calcination, and consistent with Zhou Kaiwen's research [18]. It can be seen in the Fig. 3 that the diffraction peak of sample is sharper when calcining temperature is 700 ℃ as compared to the diffraction peak obtained at 800 ℃.

3.3. FT-IR spectrum analysis

Fig. 4 shows the infrared transmission spectrum of $La_{1-x}Sr_xFeO_3$(x=0÷0.7) sample calcined at 700 ℃ for 2 h.

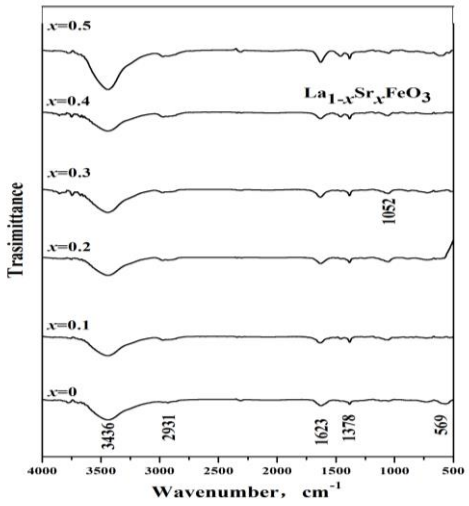

Fig. 4. FT-IR spectrum of $La_{1-x}Sr_xFeO_3$ (x = 0÷0.7) sample calcined at 700 ℃ for 2 h

The figure shows that, the main band at about 569 cm^{-1} represents Fe-O-Fe bond antisymmetric stretching vibration in the FeO_6 regular octahedron [16, 19]. This result agrees well with the result presented in [14]. Wang *et al.* [14] found that the vibrational band of Fe-O stretching appears at about 537.75 ~ 577.80 cm^{-1}. The main band Fe-O-Fe vibrational stretching bands of the spectral absorption figure of the samples as represented by Li *et al.* [20] are around the 574 cm^{-1} and 400 cm^{-1}, respectively. Few other recent publications indicate that the symmetric stretching vibration of carbonate is near 1052 cm^{-1} [18]. While 1378 cm^{-1} represents a small vibration peak corresponding to asymmetric stretching vibration of the metal [21 – 23], and 1623 cm^{-1} is indicative of the vibration derived from the asymmetric stretching vibration of carboxyl root, while Thirumalairajan *et al.* [24], found the vibrational band near 1627 cm^{-1}. Around 2931 cm^{-1}, there is a very small CO_2 absorption band. Thirumalairajan *et al.* [25] represented a similar vibrational band at about 2924 cm^{-1}. The broad peak at about 3436 cm^{-1} represents the symmetric and asymmetric stretching vibration of water molecules [26], while correlation vibration of the water molecule is represented between 3300 cm^{-1} and 3700 cm^{-1} [17, 27].

Table 2. The lattice parameter of $La_{0.9}Sr_{0.1}FeO_3$ sample calcined at different temperatures

Temperature, ℃	a, Å	b, Å	c, Å	vol, $Å^3$	Density, g/cm^3	FWHM	Crystallite, nm
uncalcined	5.57429	7.8671	5.55015	243.39	6.6246	0.423	19.3
500	5.56045	7.8621	5.56495	243.28	6.6276	0.397	20.7
700	5.55335	7.8659	5.5596	242.86	6.6392	0.308	26.4
800	5.55394	7.8657	5.56274	243.01	6.6350	0.351	23.0

3.4. Structures and grain sizes

The scanning electron microscopy (SEM) images of $La_{1-x}Sr_xFeO_3$ samples (x = 0, 0.1, 0.4) that were calcined at 700 ℃ for 2 h, is presented in Fig. 5. It can be seen from the diagram that the sample particles are ball shaped [3]. Additionally, it was also found that when the doping amount is (x = 0.1), there occurs uniform particle size distribution and good dispersion and even the surface of the particles appears to be smooth. These results were found in coherence with those obtained by Zhao *et al*. [14]. Furthermore, it has also been established that when the doping amount is (x = 0.4), particle size decreases, sample density increases and porosity of appearance reduces gradually [7, 28, 29]. When the samples were exposed to three alternating reducing and oxidizing atmospheres, the oxygen carriers showed slight agglomeration behaviour [14].

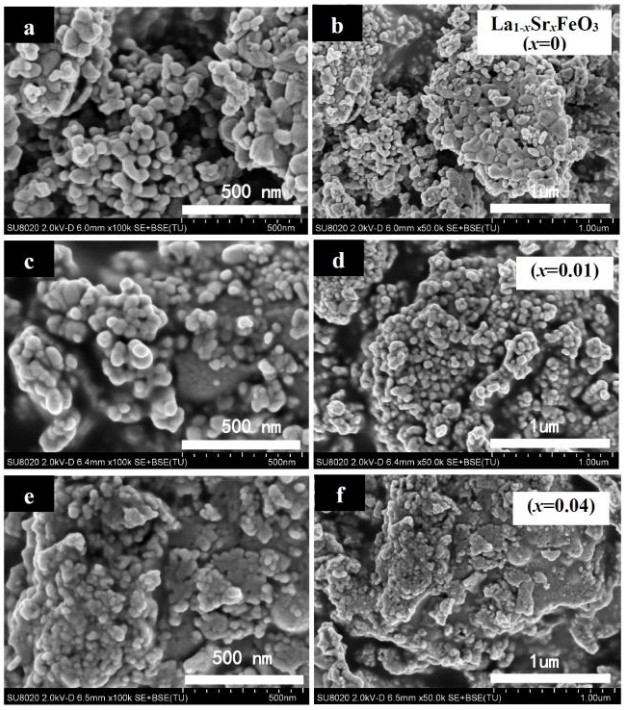

Fig. 5. SEM images of $La_{1-x}Sr_xFeO_3$ samples (x = 0, 0.1, 0.4), calcined at 700 ℃ for 2 h

Fig. 6 presents the particle size histogram of $La_{1-x}Sr_xFeO_3$ samples (x = 0,0.1,0.4) calcined at 700 ℃ for 2 h. According to the results obtained from statistical analysis of the particle size distribution, the particle size of un-doped samples was mainly concentrated in 28-68.8 nm range. As the Sr ion content changes (x=0.1), the particle size also gets modified and get concentrated in the 26-57 nm range; when it is the content (x=0.4), the particle size lies in the 21.4-35.6 nm range. These results are indicative of the fact that increase in Sr content causes decrease in particle size. The established trend of change of average grain size is consistent with Jader 5.0 software statistics and distribution analysis software statistics.

Fig. 7 represents the SEM images of $La_{0.9}Sr_{0.1}FeO_3$ samples calcined at 700 ℃, 800 ℃ for 2 h. It was found that when the calcination temperature is 700 ℃, there occurs uniform particle size distribution and dispersion. The shape of the particles is circular with visibly distinct grain boundaries, and the diffraction peak of sample is sharper when calcining temperature is 700 ℃ in Fig. 3.

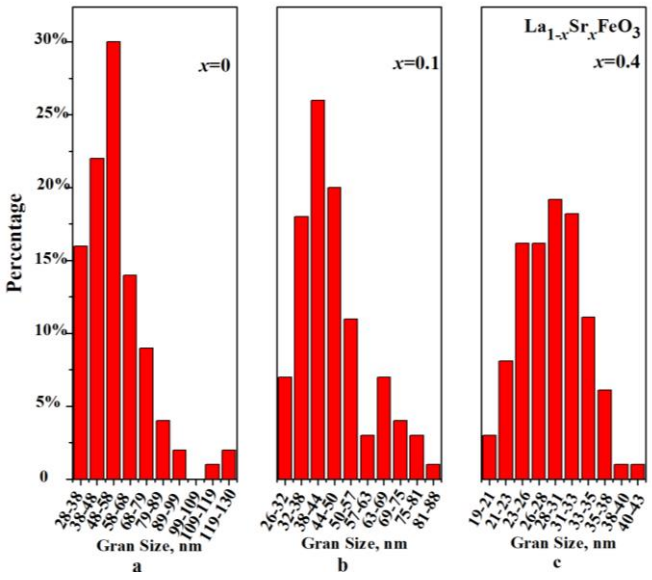

Fig. 6. Particle size histogram of $La_{1-x}Sr_xFeO_3$ samples (x=0, 0.1, 0.4) calcined at 700 ℃ for 2 h

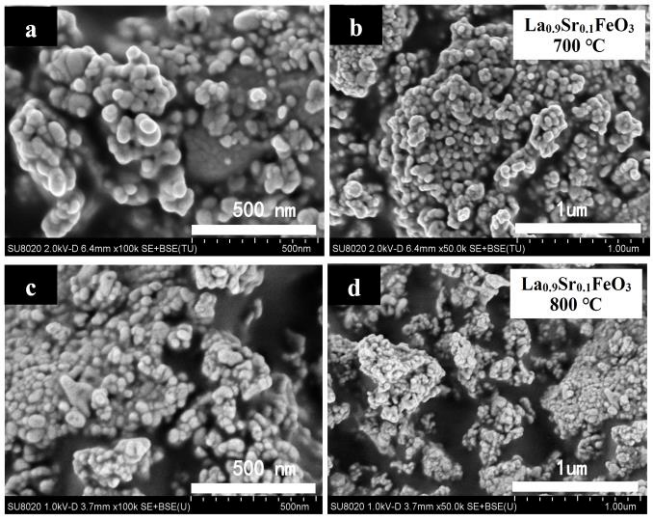

Fig. 7. SEM of $La_{0.9}Sr_{0.1}FeO_3$ samples calcined at different temperatures

Analysis of the particles when the particles are treated at 800 ℃ showed that they gradually turn crystalline during which their grain shape remain spherical, but particle size decreases, and grain boundary becomes fuzzy, reunion is more serious. These modifications are most likely the outcome of exposure to high calcining temperature that increases the chemical stress between the crystals and, causes them to shrink together [15, 30]. When the relative outcomes of exposure to different temperatures are compared it can be realized that temperature that induces calcination has the most profound influence on the morphology of the sample.

3.5. Magnetic properties of the particles

Fig. 8 represents the hysteresis loop of non-calcined $La_{1-x}Sr_xFeO_3$ samples (x = 0, 0.4, 0.7). All data presented in the figure were measured at room temperature and the

strength of the applied magnetic field was 0.8T. It is well known that ferrite $LaFeO_3$ has a G type antiferromagnetic structure, which is adjacent to the Fe^{3+} through the intermediate O^{2-} antiferromagnetic coupling. Since, the eight surface along the c axis of FeO_6 is tilted, it lies perpendicular to the antiferromagnetic direction. Due to this, the compound has a weak iron magnetic component that further results in weak ferromagnetism [5, 26]. The size of the weak ferromagnetic component is closely related to the strength of the super exchange interaction between Fe-O-Fe. The magnitude of the exchange action depends on the degree of overlap between the d orbitals of the iron atom and the p orbitals of the oxygen atom and the angle between the Fe-O-Fe [31, 32]. Combined analysis of the data presented in Fig. 8 and Table 3 indicates that magnetization increases with increasing Sr^{2+} ion concentration. This may be due to the fact that increase in concentration may cause the Sr^{2+} ions to replace La^{3+} ions [33, 34].

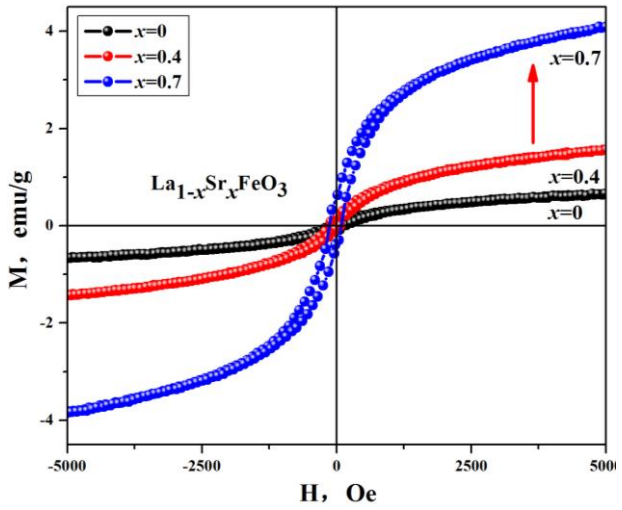

Fig. 8. Hysteresis loop of $La_{1-x}Sr_xFeO_3$ samples (x = 0, 0.4, 0.7)

In such condition, Fe^{4+} ions are formed to balance the overall electrical charge of the particles, which in turn enhances the ferromagnetic interaction between Fe^{3+} and Fe^{4+} ions [5, 35]. The substitution of La^{2+} ion by Sr^{2+} ion causes the transformation of certain fraction of Fe^{3+} to Fe^{4+} and the appearance of oxygen vacancies [36]. This can be explained by the fact that as Sr^{2+} concentration increases, Fe^{3+} (ionic radius – 0.0645 nm) gets oxidized to Fe^{4+} (ionic radius – 0.0585 nm) so that the electrically neutral nature of the whole compound is maintained [2]. Another reason is that Sr^{2+} ions decreases the grain size and increases the spin magnetic moment of the surface, so that the magnetic properties of the samples are improved [26, 33].

Table 3. Magnetic parameter of non-calcined $La_{1-x}Sr_xFeO_3$ samples (x = 0, 0.4, 0.7)

Content, x	0	0.4	0.7
Ms, emu/g	0.70	1.69	4.34
Mr, emu/g	0.05	0.14	0.50
Hc, Oe	145.95	109.49	110.49

4. CONCLUSIONS

The citrate sol-gel method with precise control and easy operation was proposed for the low temperature synthesis of Sr^{2+} ions doped $LaFeO_3$ nanoparticles. The structure, composition and magnetic properties of the nanoparticles thus formed were also studied. The TG-DTA data indicated towards the slow weightlessness of the nanoparticles as the temperature rose from 30 ℃ to 228 ℃. It was also found that 228 ℃ is the crystallization temperature of $La_{0.9}Sr_{0.1}FeO_3$ sample. The results obtained from XRD analysis showed that Sr^{2+} instead of perovskite La are responsible for the lattice forming solid solution $La_{1-x}Sr_xFeO_3$, which has a single orthogonal perovskite structure, space group Pnma and does not show any impurity peaks. When $x \leq 0.5$, the cell volume and average grain size were found to decrease with the increase of Sr doping concentration. FT-IR infrared spectrum diffraction diagram confirmed the presence of functional groups in the sample. Further analysis revealed that the antisymmetric stretching vibration of the main band at about 569 cm^{-1} is due to the presence of Fe-O-Fe in the FeO_6 regular octahedron. SEM analysis substantiated that introduction of Sr ions inhibits the growth of the particles which results in the formation of particles with spherical shape and with better morphology and dispersion properties. VSM measurements showed that $La_{1-x}Sr_xFeO_3$ is weakly ferromagnetic. Furthermore, analysis, increase of Sr^{2+} ion concentration tends to increase the magnetic properties of the sample. Finally, it was concluded that the main factors that affect the coercivity of the samples are: magnetic anisotropy, grain size, micro strain, stress, crystal symmetry, spin-orbit coupling effect, magnetic single domain size, impurities and calcination temperature.

Acknowledgments

This work was financially supported by the National Natural Science Foundation of China (NO.11364004, 11164002).F.Yang and X.X.Yang contributed equally to this work. Q. Lin and Y. He participated in experimental design. F.Yang and X.X.Yang performed the experiments. Q.Lin,H.Yang and R.J.Wang collects data. Q.Lin and Y.He are co-corresponding authors contributed equally to this study. All authors discussed the results and commented on the manuscript. The project was funded by Guangxi Key Laboratory of Nuclear Physics and Nuclear Technology.

REFERENCES

1. **Iervolino, G., Vaiano, V., Sannino, D., Rizzo, L., Palma, V.** Enhanced Photocatalytic Hydrogen Production From Glucose Aqueous Matrices on Ru-Doped $LaFeO_3$ *Applied Catalysis B Environmental* 207 2017: pp. 182 – 194. https://doi.org/10.1016/j.apcatb.2017.02.008
2. **Cyza, A., Kopia, A., Łkasz, C., Kusiński, J.** Structural Characterization of Sr Doped $LaFeO_3$, Thin Films Prepared by Pulsed Electron Deposition Method *Materials Today Proceedings* 3 (8) 2016: pp. 2707 – 2712. https://doi.org/10.1016/j.matpr.2016.06.017

3. **Elshof, J.E.T., Bouwmeester, H.J.M., Verweij, H.** Oxygen Transport Through $La_{1-x}Sr_xFeO_{3-\delta}$ Membranes II. Permeation in air/CO, CO_2 Gradients *Solid State Ionics* 89 (1 – 2) 1996: pp. 81 – 92. https://doi.org/10.1016/0167-2738(96)00255-X
4. **Zhang, X., Huaju, L.I., Yong, L.I., Shen, W.** Structural Properties and Catalytic Activity of Sr-Substituted $LaFeO_3$ Perovskite *Chinese Journal of Catalysis* 33 2012: pp. 1109 – 1114. https://doi.org/10.1016/S1872-2067(11)60388-4
5. **Liu, Z.Q., Leusink, D.P., Lü, W.M., Wang, X., Yang, X.P., Gopinadhan, K., Lin, Y.T., Annadi, A., Zhao, Y.L., Roy Barman, A., Dhar, S., Feng, Y.P., Su, H.B., Xiong, G., Venkatesan, T., Ariando.** Reversible Metal-Insulator Transition in $LaAlO_3$ Thin Films Mediated by Intragap Defects: An Alternative Mechanism for Resistive Switching *Physical Review B* 84 (16) 2011: pp. 165106. https://doi.org/10.1103/PhysRevB.84.165106
6. **Cyza, A., Cieniek, Ł., Kopia, A.** Perovskite $La_{1-x}Sr_xFeO_3$ Thin Films Deposited by Laser Ablation Process *Archives of Metallurgy Materials* 61 (2) 2016: pp. 1063 – 1067. https://doi.org/10.1515/amm-2016-0179
7. **Nakatsugawa, H., Kubota, M., Saito, M.** P-Type Thermoelectric Properties of $Pr_{1-x}Sr_xMnO_3$ $(0.1 \le x \le 0.3)$ and $La_{1-x}Sr_xFeO_3$ $(0.1 \le x \le 0.3)$ *Journal of the Japan Institute of Metals* 79 (11) 2015: pp. 597 – 606. https://doi.org/10.2320/jinstmet.JA201516
8. **Liu, Z.Q., Lü, W.M., Wang, X., Huang, Z., Annadi, A., Zeng, S.W., Venkatesan, T., Ariando.** Magnetic-field Induced Resistivity Minimum with In-Plane Linear Magnetoresistance of the Fermi Liquid In $SrTiO_{3-x}$ Single Crystals *Physical Review B* 85 (15) 2012: pp. 155114. https://doi.org/10.1103/PhysRevB.85.155114
9. **Qi, X., Zhou, J., Yue, Z., Gui, Z., Li, L.** Auto-combustion Synthesis of Nanocrystalline $LaFeO_3$ *Materials Chemistry and Physics* 78 2002: pp. 25 – 29. https://doi.org/10.1016/S0254-0584(02)00341-3
10. **Li, F.T., Liu, Y., Liu, R.H., Sun, Z.M., Zhao, D.S., Kou, C.G.** Preparation of Ca-doped $LaFeO_3$ Nanopowders in a Reverse Microemulsion and their Visible Light Photocatalytic Activity *Materials Letters* 64 2010: pp. 223 – 225. https://doi.org/10.1016/j.matlet.2009.10.048
11. **Wang, Y., Zhu, J., Zhang, L., Yang, X., Lu, L., Wang, X.** Preparation and Characterization of Perovskite $LaFeO_3$ Nanocrystals *Materials Letters* 60 2006: pp. 1767 – 1770. https://doi.org/10.1016/j.matlet.2005.12.015
12. **Shabbir, G., Qureshi, A.H., Saeed, K.** Nano-crystalline $LaFeO_3$ Powders Synthesized by the Citrate-Gel Method *Materials Letters* 60 2004: pp. 3706 – 3709. https://doi.org/10.1016/j.matlet.2006.03.093
13. **Qi, X., Zhou, J., Yue, Z., Gui, Z., Li, L.** A Simple Way to Prepare Nanosized $LaFeO_3$ Powders at Room Temperature *Ceramics International* 29 2003: pp. 347 – 349. https://doi.org/10.1016/S0272-8842(02)00119-0
14. **Zhao, K., He, F., Huang, Z., Zheng, A., Li, H., Zhao, Z.** $La_{1-x}Sr_xFeO_3$ Perovskites as Oxygen Carriers for the Partial Oxidation of Methane to Syngas *Chinese Journal of Catalysis* 35 (7) 2014: pp. 1196 – 1205. https://doi.org/10.1016/S1872-2067(14)60084-X
15. **Khomchenko, V.A., Kiselev, D.A., Vieira, J.M., Jian, L., Kholkin, A.L., Lopes, A.M.L., Pogorelov, Y.G., Araujo, J.P., Maglione, M.** Effect of Diamagnetic Ca, Sr, Pb, and Ba Substitution on the Crystal Structure and Multiferroic Properties of the $BiFeO_3$ Perovskite *Journal of Applied Physics* 103 (2) 2008: pp. 024105. https://doi.org/10.1063/1.2836802
16. **Wang, C., Shaw, L.L.** On Synthesis of Fe_2SiO_4/SiO_2 and Fe_2O_3/SiO_2, Composites through Sol-Gel and Solid-State Reactions *Journal of Sol-Gel Science and Technology* 72 (3) 2014: pp. 602 – 614. https://doi.org/10.1007/s10971-014-3483-5
17. **Lebid, M., Omari, M.** Synthesis and Electrochemical Properties of $LaFeO_3$ Oxides Prepared via Sol-Gel Method *Arabian Journal for Science and Engineering* 39 2014: pp. 147 – 152. https://doi.org/10.1007/s13369-013-0883-8
18. **Zhou, K., Wu, X., Wu, W., Xie, J., Tang, S., Liao, S.** Nanocrystalline $LaFeO_3$ Preparation and Thermal Process of Precursor *Advanced Powder Technology* 24 2013: pp. 359 – 363. https://doi.org/10.1016/j.apt.2012.08.009

    Azab, A.A., Helmy, N., Albaaj, S. Structural and Magnetic Properties of $La_{1-x}Ce_xFe_{1-x}Cr_xO_3$ Orthoferrite Prepared by Co-Precipitation Method *Materials Research Bulletin* 66 2015: pp. 249 – 253. https://doi.org/10.1016/j.materresbull.2015.02.038
19. **Li, S., Jing, L., Fu, W., Yang, L., Xin, B., Fu, H.** Photoinduced Charge Property of Nanosized Perovskite-Type $LaFeO_3$ and its Relationships with Photocatalytic Activity Under Visible Irradiation *Materials Research Bulletin* 42 2007: pp. 203 – 212. https://doi.org/10.1016/j.materresbull.2006.06.010
20. **Abazari, R., Sanati, S., Saghatforoush, L.A.** A Unique and Facile Preparation of Lanthanum Ferrite Nanoparticles in Emulsion Nanoreactors Morphology, Structure, and Efficient Photocatalysis *Materials Science in Semiconductor Processing* 25 2014: pp. 301 – 306. https://doi.org/10.1016/j.mssp.2014.01.017
21. **Feng, J., Liu, T., Xu, Y., Zhao, J., He, Y.** Effects of PVA Content on the Synthesis of $LaFeO_3$ via Sol-Gel Route *Ceramics International* 37 2011: pp. 1203 – 1207. https://doi.org/10.1016/j.ceramint.2010.11.045
22. **Abazari, R., Sanati, S.** Perovskite $LaFeO_3$ Nanoparticles Synthesized by the Reverse Microemulsion Nanoreactors in the Presence of Aerosol-ot: Morphology, Crystal Structure, and their Optical Properties Superlattices and Microstructures 64 2013: pp. 148 – 157. https://doi.org/10.1016/j.spmi.2013.09.017
23. **Thirumalairajan, S., Girija, K., Ganesh, I., Mangalaraj, D., Viswanathan, C., Balamurugan, A., Ponpandian, N.** Controlled Synthesis of Perovskite $LaFeO_3$ Microsphere Composed of Nanoparticles via Self-Assembly Process and their Associated Photocatalytic Activity *Chemical Engineering Journal* 209 2012: pp. 420 –428. https://doi.org/10.1016/j.cej.2012.08.012
24. **Thirumalairajan, S., Girija, K., Ganesh, V., Mangalaraj, D., Viswanathan, C., Ponpandian, N**. Novel Synthesis of $LaFeO_3$ Nanostructure Dendrites a Systematic Investigation of Growth Mechanism, Properties, and Biosensing for Highly Selective Determination of Neurotransmitter Compounds *Crystal Growth & Design* 13 2013: pp. 291 – 302. https://doi.org/10.1021/cg3014305
25. **Janbutrach, Y., Hunpratub, S., Swatsitang, E.** Ferromagnetism and Optical Properties of $La_{1-x}Al_xFeO_3$ Nanopowders *Nanoscale Research Letters* 9 (1) 2014: pp. 498.

https://doi.org/10.1186/1556-276X-9-498

26. **Ciambelli, P., Cimino, S., Rossi, S.D., Lisi, L., Minelli, G., Porta, P., Russo, G.** $AFeO_3$ (A=La, Nd, Sm) and $LaFe_{1-x}Mg_xO_3$ Perovskites as Methane Combustion and CO Oxidation Catalysts Structural, Redox and Catalytic Properties *Applied Catalysis B: Environmental* 29 2001: pp. 239 – 250. https://doi.org/10.1016/S0926-3373(00)00215-0
27. **Lin, Q., Lin, J., He, Y., Wang, R., Dong, J.** The Structural and Magnetic Properties of Gadolinium Doped $CoFe_2O_4$ Nanoferrites *Journal of Nanomaterials* 2015: pp. 294239. https://doi.org/10.1155/2015/294239
28. **Shikha, P., Kang, T.S., Randhawa, B.S. Preet Shikha, Tejwant Singh Kang, B.S. Randhawa**. Effect of Different Synthetic Routes on the Structural, Morphological and Magnetic Properties of Ce doped $LaFeO_3$ Nanoparticles *Journal of Alloys and Compounds* 625 2015: pp. 336 – 345. https://doi.org/10.1016/j.jallcom.2014.11.074
29. **Gryaznov, D., Merkle, R., Kotomin, E.A., Maier, J.** Ab Initio Modelling of Oxygen Vacancies and Protonic Defects in $La_{1-x}Sr_xFeO_{3-\delta}$ Perovskite Solid Solutions *Journal of Materials Chemistry A* 4 (34) 2016: pp. 13093 – 13104. https://doi.org/10.1039/C6TA04109D
30. **Liu, Z.Q., Lu, W.M., Lim, S.L., Qiu, X.P., Bao, N.N., Motapothula, M., Yi, J.B., Yang, M., Dhar, S., Venkatesan, T., Ariando.** Reversible Room-Temperature Ferromagnetism in Nb-doped $SrTiO_3$ Single Crystals *Physical Review B* 87 (22) 2013: pp. 220405. https://doi.org/10.1103/PhysRevB.87.220405
31. **Islam, M.A., Xie, Y., Scafetta, M.D., May, S.J., Spanier, J.E.** Raman Scattering in $La_{1-x}Sr_xFeO_{3-\delta}$ Thin Films: Annealing-Induced Reduction and Phase Transformation *Journal of Physics Condensed Matter* 27 (15) 2015: pp. 155401. https://doi.org/10.1088/0953-8984/27/15/155401
32. **Li, J., Xinli, K., Yong, Q., He, H.** Microstructure and Magnetic Properties of $La_{1-x}Sr_xFeO_3$ Nanoparticles *Physica Status Solidi* 191 (1) 2002: pp. 255 – 259. https://doi.org/10.1002/1521-396X(200205)191:1<255::AID-PSSA255>3.0.CO;2-N
33. **Bongio, E.V., Black, H., Raszewski, F.C., Edwards, D., Mcconville, C.J., Amarakoon, V.R.W.** Microstructural and High-Temperature Electrical Characterization of $La_{1-x}Sr_xFeO_{3-\delta}$ *Journal of Electroceramics* 14 (3) 2005: pp. 193 – 198. https://doi.org/10.1007/s10832-005-0957-4
34. **Lin, J., He, Y., Lin, Q., Wang, R., Chen, H.** Microstructural and Mössbauer Spectroscopy Studies of $Mg_{1-x}Zn_xFe_2O_4$ (x = 0.5, 0.7) Nanoparticles *Journal of Spectroscopy* 2014: pp. 540319. https://dx.doi.org/10.1155/2014/540319
35. **Mandal, S.K., Rakshit, T., Ray, S.K., Mishra, S.K., Krishna, P.S., Chandra, A.** Nanostructures of Sr^{2+} Doped $BiFeO_3$ Multifunctional Ceramics with Tunable Photoluminescence and Magnetic Properties *Journal of Physics: Condensed Matter* 25 (5) 2013: pp. 055303. https://doi.org/10.1088/0953-8984/25/5/055303